

**SYNTHESIS AND CHARACTERISATION OF
N-DOPED GRAPHENE QUANTUM
DOTS/TITANIUM DIOXIDE NANOCOMPOSITE
AS PHOTOSENSITISER IN PHOTODYNAMIC
THERAPY FOR BREAST CANCER TREATMENT**

PRAVENA A/P RAMACHANDRAN

UNIVERSITI SAINS MALAYSIA

2021

**SYNTHESIS AND CHARACTERISATION OF
N-DOPED GRAPHENE QUANTUM
DOTS/TITANIUM DIOXIDE NANOCOMPOSITE
AS PHOTOSENSITISER IN PHOTODYNAMIC
THERAPY FOR BREAST CANCER TREATMENT**

by

PRAVENA A/P RAMACHANDRAN

**Thesis submitted in fulfilment of the requirements
for the degree of
Master of Science**

March 2021

ACKNOWLEDGEMENT

First and foremost, praises and thanks to God, the Almighty, for His blessings and graces. My special thanks to the School of Chemical Sciences and Institute of Postgraduate Studies (IPS), Universiti Sains Malaysia (USM) for allowing me to conduct my research work in fulfilment of my Master's degree. I would like to express my sincere gratitude to my research supervisor Dr Lee Hooi Ling for her continuous assistance, encouragement and providing invaluable guidance throughout this project. I am grateful to my Co-supervisor Dr Lee Chong Yew for his helpful suggestions and valuable input. I also sincerely acknowledge the Yayasan Tan Sri Lee Shin Cheng and Research University (Individual) (RUI) Grant Scheme (1001/PKIMIA/8011086) from IOI Group and Universiti Sains Malaysia, respectively, for the financial support. My appreciation also extends to all our research collaborators Prof. Ruey-An Doong (National Tsing Hua University, Taiwan) for helping me to conduct HRTEM and XPS analysis, Assoc. Prof. Dr Oon Chern Ein (INFORMM, USM) for providing me with the breast cancer cells, Assoc. Prof. Dr Vikneswaran Murugaiyah (School of Pharmaceutical Sciences, USM) for his insightful comments and guidance. My special appreciation to all my friends for helping me with this project, especially, Khor Boon Keat, Hanisah, Vicinisvarri, Athira, Izzati, Stephen and Triguna. Not forgetting, the technical staff from School of Chemical Sciences and School of Pharmaceutical Sciences for providing the facilities and assistance. Last but not least, I am thankful to the most precious people in my life, my parents, Mr. and Mrs. Ramachandran Parimala and my siblings, Kanchana, Ragurajan and Ramakrishnan for their love, sacrifices and unconditional support throughout my MSc journey.

TABLE OF CONTENTS

ACKNOWLEDGEMENT	ii
TABLE OF CONTENTS	iii
LIST OF TABLES	ix
LIST OF FIGURES	xi
LIST OF SCHEMES	xvii
LIST OF SYMBOLS	xviii
LIST OF ABBREVIATIONS	xix
LIST OF APPENDICES	xxi
ABSTRAK	xxii
ABSTRACT	xxiv
CHAPTER 1 INTRODUCTION	1
1.1 Overview	1
1.2 Problem Statement	5
1.3 Research objectives	6
1.4 Outline of thesis	6
CHAPTER 2 LITERATURE REVIEW	8
2.1 Nanotechnology in biomedical applications	8
2.2 Nanomaterials in photodynamic therapy	12
2.3 Titanium dioxide (TiO ₂)	15
2.3.1 General	15
2.3.2 Chemical structure and properties	15
2.3.3 Application of TiO ₂ in the biomedical field	19
2.4 Modification of TiO ₂ into TiO ₂ nanocomposites	22
2.5 Combination of TiO ₂ with quantum dots	27

2.6	Graphene Quantum Dots (GQDs)	28
2.6.1	Properties of GQDs	28
2.6.2	Nitrogen-doping of GQDs (N-GQDs)	30
2.6.3	GQDs as a potential photosensitiser and nanocarrier for photosensitisers in PDT	35
2.7	Summary	40
CHAPTER 3 MATERIALS AND EXPERIMENTAL METHODS		41
3.1	Introduction	41
3.2	Materials	41
3.3	Experimental methods	42
3.3.1	Synthesis of N-GQDs	42
3.3.1(a)	Effect of the molar ratio of precursors	42
3.3.1(b)	Effect of temperature	43
3.3.1(c)	Effect of hydrothermal treatment duration	43
3.3.1(d)	Effect of different types of nitrogen precursors	43
3.3.2	Synthesis of titanium dioxide nanoparticles (TiO ₂ NPs)	44
3.3.2(a)	Effect of initial solution pH	44
3.3.2(b)	Effect of reaction time	44
3.3.2(c)	Effect of microwave power	45
3.3.3	Synthesis of N-GQDs/TiO ₂ NCs	45
3.3.4	Quantum yield calculations	46
3.3.5	Position of conduction band calculations	46
3.4	Experimental setup for photodynamic treatment	47
3.4.1	Cell culture and the conditions	47
3.4.2	Nanoparticle preparation and exposure to cells	48
3.4.3	Cytotoxicity assay	48

3.4.4	Photokilling effects of N-GQDs/TiO ₂ NCs on MDA-MB-231 and HS27 cells	49
3.4.5	Measurement of reactive oxygen species (ROS) level	50
3.4.5(a)	Measurement of intracellular ROS level	50
3.4.5(b)	Measurement of specific types of ROS	51
3.4.6	Measurement of Caspase-3/7 activity	52
3.4.7	Measurement of mitochondrial activity	52
3.4.8	Statistical analysis	53
3.5	Sample characterisations	53
3.5.1	Fourier transform infrared (FTIR) spectroscopy	53
3.5.2	Ultraviolet-Visible (UV-Vis) spectroscopy	54
3.5.3	Photoluminescence (PL) spectroscopy	55
3.5.4	X-Ray diffraction (XRD)	56
3.5.5	Field emission scanning electron microscopy (FESEM) and scanning electron microscopy (SEM) with energy-dispersive X-ray (EDX)	57
3.5.6	High-resolution transmission electron microscopy (HRTEM) and selected area electron diffraction (SAED)	57
3.5.7	X-ray photoelectron spectroscopy (XPS)	58
3.5.8	Dynamic light scattering (DLS)	58
3.6	Experimental Approach	59
CHAPTER 4 SYNTHESIS AND CHARACTERISATION OF N-GQDS, TiO₂ NANOPARTICLES AND N-GQDS/TiO₂ NANOCOMPOSITES		61
4.1	Introduction	61
4.2	Synthesis and characterisations of N-GQDs	61
4.2.1	Optimisation of N-GQDs	61
4.2.1(a)	Effect of the molar ratio of precursors	62
4.2.1(b)	Effect of temperature	64

	4.2.1(c) Effect of hydrothermal treatment duration	65
	4.2.1(d) Effect of different types of nitrogen precursors	67
4.2.2	Characterisation of N-GQDs	68
	4.2.2(a) Fourier transform infrared (FTIR) spectroscopy	68
	4.2.2(b) X-ray diffraction (XRD)	71
	4.2.2(c) High-Resolution Transmission Electron Microscope (HRTEM)	73
	4.2.2(d) Optical properties of N-GQDs	74
4.2.3	Possible formation mechanism of N-GQDs	77
4.3	Synthesis and characterisations of TiO ₂ NPs	78
	4.3.1 Optimisation of TiO ₂ NPs	78
	4.3.1(a) Effect of initial solution pH	78
	4.3.1(b) Effect of reaction time	80
	4.3.1(c) Effect of microwave power	82
	4.3.2 Characterisations of synthesised TiO ₂ NPs	84
	4.3.2(a) Fourier transform infrared (FTIR) spectroscopy	84
	4.3.2(b) UV-Visible diffuse reflectance spectroscopy (UV-Vis DRS)	86
	4.3.2(c) Field emission scanning electron microscopy (FESEM)	88
	4.3.2(d) High-Resolution Transmission Electron Microscope (HRTEM)	89
	4.3.2(e) X-ray photoelectron spectroscopy (XPS)	90
	4.3.3 Possible formation mechanism of TiO ₂ NPs	95
4.4	Synthesis and characterisations of N-GQDs/TiO ₂ NCs	97
	4.4.1 Characterisations of synthesised N-GQDs/TiO ₂ NCs	97
	4.4.1(a) X-ray diffraction (XRD)	97
	4.4.1(b) Fourier transform infrared (FTIR)	99

4.4.1(c)	UV-Visible diffuse reflectance spectroscopy (UV-Vis DRS)	101
4.4.1(d)	Field Emission Scanning Electron Microscope (FESEM)	103
4.4.1(e)	High-Resolution Transmission Electron Microscope (HRTEM)	104
4.4.1(f)	X-ray photoelectron spectroscopy (XPS)	106
4.4.2	Possible formation mechanism of Ti-O-C bond of N-GQDs/TiO ₂ NCs	109
4.4.3	Summary	111
CHAPTER 5 PHOTODYNAMIC ACTIVITY OF N-GQDs/TiO₂ NCs ON MDA-MB-231 CELL LINE		113
5.1	Introduction	113
5.2	N-GQDs, TiO ₂ NPs and N-GQDs/TiO ₂ NCs administration in cell culture media and their in vitro cytotoxicity assessment using the MDA-MB-231 breast cancer cell line and HS27 human fibroblast cell line	114
5.2.1	Characterisation of N-GQDs, TiO ₂ NPs and N-GQDs/TiO ₂ NCs in cell culture media	114
5.2.2	<i>In vitro</i> cytotoxicity assessment of N-GQDs, TiO ₂ NPs and N-GQDs/TiO ₂ NCs using the MDA-MB-231 breast cancer cell line and HS27 human fibroblast cell line	121
5.3	Photodynamic activity of N-GQDs/TiO ₂ NCs on MDA-MB-231	127
5.3.1	<i>In vitro</i> photokilling effects of N-GQDs/TiO ₂ NCs on MDA-MB-231	127
5.3.2	Selectivity of the treatment	131
5.3.3	Production of Reactive Oxygen Species (ROS)	133
	5.3.3(a) Intracellular ROS levels	133
	5.3.3(b) Specific types of ROS	135
5.3.4	Apoptosis	139
5.3.5	Mitochondrial activity	142
5.4	Summary	144

CHAPTER 6	CONCLUSIONS AND FUTURE WORK	
	RECOMMENDATIONS	146
6.1	Conclusions	146
6.2	Recommendations for future studies	149
	REFERENCES	150
	APPENDICES	
	LIST OF PUBLICATIONS	

LIST OF TABLES

	Page
Table 2.1	TiO ₂ NPs synthesis method, reaction conditions and their respective outcome 18
Table 2.2	TiO ₂ based nanocomposite applied in PDT reaction for treating various cancer cells 25
Table 2.3	Methods for synthesising N-GQDs, reaction conditions and respective quantum yield 34
Table 2.4	Nanoparticles in PDT application for breast cancer cells 38
Table 3.1	Varied molar ratio between the ethylenediamine and citric acid for the synthesis of N-GQDs 43
Table 4.1	Crystallite size and lattice parameters of TiO ₂ NPs prepared using different initial solution pH 80
Table 4.2	Crystallite size, lattice parameters and lattice strain of TiO ₂ NPs prepared at different reaction time 82
Table 4.3	Crystallite size and lattice parameters of TiO ₂ NPs prepared at different microwave power irradiation 84
Table 4.4	The binding energy (eV) data obtained from XPS analysis of Ti 2p spectrum. The spectra were corrected using C 1s line at 284.6 eV 93
Table 4.5	The binding energy (eV) data obtained from XPS analysis of O 1s and C1s spectra. The spectra were corrected using C 1s line at 284.6 eV 94
Table 4.6	Crystallite size, lattice parameters and lattice strain of N-GQDs/TiO ₂ NCs prepared using different amounts of TTIP loading and synthesised TiO ₂ NPs 99

Table 4.7	The binding energy (eV) data obtained from XPS analysis of Ti 2p, O 1s, C 1s and N 1s spectra. The spectra were corrected using C 1s line at 284.6 eV 109
Table 5.1	Dispersing parameters of N-GQDs, TiO ₂ NPs, N-GQDs/TiO ₂ NCs in cell culture medium (mean ± SD, n=3). The nanomaterials were dispersed in water or medium with or without FBS (5 or 1%, v/v), then sonicated, vortexed and hydrodynamic size and zeta potential were measured 120
Table 5.2	Types of ROS percentage (%) of total ROS generated by N-GQDs/TiO ₂ NCs (0.5 mg/mL) under irradiation of NIR light for 20 min. Data represented are mean ± SD of two independent experiments made in three replicates (n=6) 136

LIST OF FIGURES

	Page
Figure 2.1	Type I and type II reaction mechanism of ROS generation in PDT 12
Figure 2.2	Bulk crystalline structures of the (a) anatase, (b) brookite and (c) rutile type TiO ₂ (Bianchi et al., 2016) 17
Figure 2.3	Different types of N atoms in the graphene lattice (Wei et al., 2009) 31
Figure 3.1	Schematic diagram for experimental setup to study the photokilling effects of nanocomposites under light irradiation 49
Figure 4.1	(a) UV-Vis spectra and (b) PL spectra of N-GQDs synthesised with different molar ratio CA:EDA at constant temperature (180 °C), reaction duration (4 h) 63
Figure 4.2	(a) UV-Vis spectra and (b) PL spectra of N-GQDs synthesised with the different temperature at constant reaction duration (4 h), molar ratio CA:EDA (1:1) 64
Figure 4.3	(a) UV-Vis spectra and (b) PL spectra of N-GQDs synthesised with different reaction duration at constant temperature (180 °C), molar ratio CA:EDA (1:1) 66
Figure 4.4	(a) UV-Vis spectra and (b) PL spectra of N-GQDs synthesised with different types of amine at constant temperature (180 °C), reaction duration (4 h), molar ratio CA:amine (1:1) 67
Figure 4.5	FTIR spectra for (a) citric acid (CA), (b) ethylenediamine (EDA), (c) synthesised N-GQDs 71
Figure 4.6	X-ray diffractograms of synthesised N-GQDs 72

Figure 4.7	(a-f) HRTEM images of N-GQDs. The insets show FFT image corresponding to selected area, (g) Particle-size distribution of N-GQDs	74
Figure 4.8	(a) UV-vis spectrum (blue line), PLE spectrum (red line) and PL emission spectrum (green line) of the N-GQDs, (b) Typical PL spectra of the N-GQDs at different excitation wavelength, (c) PL intensity and UV-vis absorbance of the N-GQDs (excited at 340 nm). The insets show photo-stability spectrum of N-GQDs and photos of the N-GQDs in aqueous solution under 400–780 nm visible light (left) and 365 nm UV light (right).....	76
Figure 4.9	Reaction mechanism of N-GQDs using citric acid and ethylenediamine	77
Figure 4.10	X-ray diffractograms of TiO ₂ NPs synthesised at 600 W, 20 min and using initial solution pH of (a) pH 9, (b) pH 7, (c) pH 1.3, (d) pH 1.3 (uncalcined).....	79
Figure 4.11	X-ray diffractograms of TiO ₂ NPs synthesised using initial solution pH of 1.3, 600 W and at (a) 5 min (b) 10 min, (c) 20 min	81
Figure 4.12	X-ray diffractograms of TiO ₂ NPs synthesised using initial solution pH 1.3, 20 min and at (a) 200 W (b) 400 W, (c) 600 W.....	83
Figure 4.13	FTIR spectra for (a) uncalcined synthesised TiO ₂ NPs, (b) calcined synthesised TiO ₂ NPs, (c) pure anatase TiO ₂	85
Figure 4.14	UV-Vis absorbance spectra TiO ₂ NPs synthesised using various initial solution pH, reaction time and microwave power. The inset shows the obtained pure white powder of synthesised TiO ₂ NPs under optimum conditions	86
Figure 4.15	Bandgap of TiO ₂ NPs synthesised using various initial solution pH, reaction time and microwave power	88
Figure 4.16	FESEM images of the synthesised TiO ₂ NPs	89

Figure 4.17	(a-e) HRTEM images (f) SAED pattern. The insets show FFT image corresponding to the selected area and particle-size distribution of TiO ₂ NPs	90
Figure 4.18	Possible formation mechanism of oxygen vacancies and Ti ³⁺ ions.....	92
Figure 4.19	Possible formation mechanism of oxygen vacancies (bridging oxygen site) and Ti ³⁺ ions <i>via</i> thermal treatment.	93
Figure 4.20	High-resolution XPS spectra of Ti 2p of synthesised TiO ₂ NPs under optimum conditions (pH 1.3, 20 min, 600 W).....	93
Figure 4.21	High-resolution XPS spectra of (a) O 1s and (b) C 1s of synthesised TiO ₂ NPs under optimum conditions (pH 1.3, 20 min, 600 W)	94
Figure 4.22	Schematic illustration of the TiO ₂ aggregates formation process.....	96
Figure 4.23	X-ray diffractograms of N-GQDs/TiO ₂ NCs synthesised using (a) 1 mL TTIP, (b) 2 mL TTIP, (c) 3 mL TTIP, (d) TiO ₂ NPs synthesised under acidic condition	98
Figure 4.24	FTIR spectra for (a) N-GQDs, (b) synthesised TiO ₂ NPs, (c) N-GQDs/TiO ₂ NCs.....	100
Figure 4.25	UV-Vis absorbance spectra of N-GQDs/TiO ₂ NCs synthesised using different amount of TTIP loading and synthesised TiO ₂ NPs. The inset shows the obtained brown coloured powder of synthesised N-GQDs/TiO ₂ NCs under optimum conditions	101
Figure 4.26	Bandgap of N-GQDs/TiO ₂ NCs synthesised using different TTIP loading and synthesised TiO ₂ NPs.....	103
Figure 4.27	FESEM images of the synthesised N-GQDs/TiO ₂ NCs	104
Figure 4.28	(a-d) HRTEM images (e) SAED pattern. The inset shows particle-size distribution of N-GQDs/TiO ₂ NCs.....	105

Figure 4.29	High-resolution XPS spectra of Ti 2p of synthesised N-GQDs/TiO ₂ NCs using 3 mL TTIP.....	106
Figure 4.30	High-resolution XPS spectra of O 1s of synthesised N-GQDs/TiO ₂ NCs using 3 mL TTIP.....	107
Figure 4.31	High-resolution XPS spectra of (a) C 1s and (b) N 1s of synthesised N-GQDs/TiO ₂ NCs using 3 mL TTIP	109
Figure 4.32	Chemical synthesis process of N-GQDs/TiO ₂ NCs	110
Figure 5.1	Brownian motion between particles and the resulting collision and adhesion between particles.....	115
Figure 5.2	Cell viability of (a) MDA-MB-231 cells after 24 h post treatment, (b) HS27 cells after 24 h post treatment, (c) MDA-MB-231 cells after 48 h post treatment, (d) HS27 cells after 48 h post treatment, respectively with N-GQDs, TiO ₂ NPs and N-GQDs/TiO ₂ NCs. Data are presented as the mean ± SD of two independent experiments made in three replicates (n = 6). Significant difference was tested using two-way ANOVA followed by Bonferroni post-hoc test as compared to control *(p < 0.05), **(p < 0.01) and ***(p < 0.001)	125
Figure 5.3	The MDA-MB-231 cells treated with different concentrations of N-GQDs/TiO ₂ NCs (0.05 – 0.5 mg/mL), then irradiated with various doses of NIR light (5 – 20 min). The cell viability was estimated at 24 h after irradiation. Data are presented as the mean ± SD of two independent experiments made in three replicates (n = 6) and normalised to control. Significant difference was tested using one-way ANOVA followed by Tukey post-hoc test as compared to control *(p < 0.05), **(p < 0.01) and ***(p < 0.001)	128
Figure 5.4	The multi-stage operation of PDT	130

Figure 5.5	The MDA-MB-231 and HS27 cells treated with different concentrations of N-GQDs/TiO ₂ NCs (0.05 – 0.5 mg/mL), then irradiated with NIR light for 20 min. The cell viability was estimated at 24 h after irradiation. Data are presented as the mean ± SD of two independent experiments made in three replicates (n = 6) and normalised to control. Significant difference was tested using two-way ANOVA followed by Bonferroni post-hoc test as compared to MDA-MB-231 *(p < 0.05), **(p < 0.01) and ***(p < 0.001).	131
Figure 5.6	ROS levels of MDA-MB-231 and HS27 cells were treated with different concentrations of N-GQDs/TiO ₂ NCs (0.05 – 0.5 mg/mL) and were irradiated with NIR light for 20 min. Data are presented as the mean ± SD of two independent experiments made in three replicates (n = 6) and normalised to control. Significant difference was tested using two-way ANOVA followed by Bonferroni post-hoc test as compared to MDA-MB-231 *(p < 0.05), **(p < 0.01) and ***(p < 0.001).	134
Figure 5.7	Comparison of photo-induced reactive oxygen species (ROS) generated by N-GQDs/TiO ₂ NCs under irradiation of NIR light as a function of irradiation time	136
Figure 5.8	A proposed possible mechanism of ROS generation by N-GQDs/TiO ₂ NCs upon NIR light irradiation	138
Figure 5.9	The morphology of cells undergoing apoptosis, necrosis and autophagy (Montaseri et al., 2020)	140

Figure 5.10 Induction of apoptosis in MDA-MB-231 cells treated with different concentrations of N-GQDs/TiO₂ NCs (0.05 – 0.5 mg/mL) and were irradiated with NIR light for 20 min. Data are presented as the mean ± SD of two independent experiments made in three replicates (n=6). Significant difference was tested using one-way ANOVA followed by Tukey post-hoc test as compared to control *(p<0.05), **(p<0.01) and ***(p<0.001)..... 142

Figure 5.11 Measurement of the mitochondrial membrane potential of MDA-MB-231 cells treated with different concentrations of N-GQDs/TiO₂ NCs (0.05 – 0.5 mg/mL) and were irradiated with NIR light for 20 min. Data are presented as the mean ± SD of three replicates (n=3) Significant difference was tested using one-way ANOVA followed by Tukey post-hoc test as compared to control *(p<0.05), **(p<0.01) and ***(p<0.001)..... 144

LIST OF SCHEMES

	Page
Scheme 3.1 Outline of the experimental approach	60

LIST OF SYMBOLS

%	Percent
°C	Degree celsius
Å	Angstrom
% T	Percent transmittance
e ⁻	Electrons
h ⁺	Holes
π	Bonding states
π*	Antibonding states
S ₀	Ground state
S _n	Excited singlet state
T ₁	Triplet state
³ O ₂	Molecular oxygen
¹ O ₂	Singlet oxygen

LIST OF ABBREVIATIONS

ATR	Attenuated total reflection
CA	Citric acid
CB	Conduction band
DCFDA	2',7'-dichlorofluorescein diacetate
DEA	Diethylamine
DI	Deionised water
DLS	Dynamic light scattering
DMEM	Dulbecco's modified eagle's medium
EDA	Ethylenediamine
EDL	Electrical double layer
EDX	Energy dispersive X-ray
eV	Electrovolt
EPR	Enhanced permeability and retention
FBS	Fetal bovine serum
FESEM	Field emission scanning electron microscope
FTIR	Fourier-transform infrared
HOMO	Highest occupied molecular orbital
HRTEM/SAED	High-resolution transmission electron microscopy with selected area electron diffraction
HS27	Human fibroblast cells
LUMO	Lowest unoccupied molecular orbital
MDA-MB-231	Human breast cancer cells
MOMP	Mitochondrial outer membrane permeabilisation

N	Nitrogen
NIR	Near-infrared
N-GQDs	N-doped graphene quantum dots
N-GQDs/TiO ₂ NCs	N-doped graphene quantum dots/titanium dioxide nanocomposites
NH ₄ OH	Ammonia solution
PDT	Photodynamic therapy
PL	Photoluminescence
QDs	Quantum dots
QS	Quinine sulfate
QY	Quantum yield
ROS	Reactive oxygen species
SD	Standard deviation
TEA	Triethylamine
TiO ₂ NPs	Titanium dioxide nanoparticles
TMRE	Tetramethylrhodamine ethyl ester
TTIP	Titanium (IV) tetraisopropoxide
UV-Vis	Ultraviolet–visible
VB	Valence band
vdW	van der Waals force
W	Watt
XPS	X-ray photoelectron spectroscopy
XRD	X-ray diffraction

LIST OF APPENDICES

APPENDIX A	EXAMPLE CALCULATION OF MOLAR RATIO OF CITRIC ACID (CA) : ETHYLENEDIAMINE (EDA)
APPENDIX B	EXAMPLE CALCULATION OF CONCENTRATION TITANIUM(IV) ISOPROPOXIDE (TTIP) USED IN THE PREPARATION OF N-GQDs/TiO ₂ NCs
APPENDIX C	EXAMPLE CALCULATION OF LATTICE PARAMETERS OF THE TiO ₂ NPs (pH 1.3, 20 min, 600 W)
APPENDIX D	EXAMPLE CALCULATION OF LATTICE STRAIN OF THE TiO ₂ NPs (pH 1.3, 20 min, 600 W)
APPENDIX E	EDX ANALYSIS OF TiO ₂ NPs (pH 1.3, 20 min, 600 W)
APPENDIX F	EDX ANALYSIS OF N-GQDs/TiO ₂ NCs (3 mL TTIP)

**SINTESIS DAN PENCIRIAN NANOKOMPOSIT N-TERDOP TITIK
KUANTUM GRAFIN/TITANIUM DIOKSIDA SEBAGAI
FOTOSENSITISER DALAM TERAPI FOTODINAMIK UNTUK
RAWATAN KANSER PAYUDARA**

ABSTRAK

Nanopartikel titanium dioksida (TiO_2 NP) telah terbukti sebagai calon yang berpotensi dalam terapi kanser, khususnya dalam aplikasi terapi fotodinamik (PDT). Walau bagaimanapun, aplikasi TiO_2 NP terhad disebabkan oleh kadar penggabungan semula pasangan elektron (e^-)/ lubang positif (h^+) yang cepat berpunca daripada jurang tenaga yang lebih luas. Oleh hal yang demikian, pengubahsuaian permukaan telah diterokai untuk menganjakkan tepi penyerapan kepada panjang gelombang cahaya yang lebih panjang untuk membolehkan penembusan ke dalam ketumbuhan yang mendalam. Dalam kajian ini, TiO_2 NP telah berkonjugat dengan N-terdop titik kuantum grafin (N-GQDs/ TiO_2 NK) untuk melanjutkan ciri-ciri penyerapan cahaya kepada panjang gelombang inframerah. Suatu kaedah mudah satu-bekas hidroterma telah digunakan untuk mensintesis N-GQDs yang mempunyai purata saiz partikel 4.40 ± 1.5 nm pada keadaan optima dengan nisbah molar asid sitrik (CA):etilenediamin (EDA) (1:1) pada 180°C untuk 4 jam dan amina primer (EDA) sebagai pelopor N. N-GQDs beremisi biru mempunyai hasil kuantum fotoluminasi (PL) 80.2 %, telah mempamerkan pengujaan-bebas pemancaran PL pada 442 nm dengan panjang gelombang pengujaan pada 340 nm. Manakala, anatase TiO_2 NP telah disintesis dengan menggunakan sintesis mikro-gelombang berbantu dalam fasa akueus dengan purata saiz partikel 11.46 ± 2.8 nm, saiz hablur yang kecil (12.2

nm) dan jurang tenaga yang rendah (2.93 eV). Berdasarkan analisis spektroskopi fotoelektron sinar-X (XPS), didapati bahawa TiO₂ NP berbentuk segi empat tepat yang telah disintesis pada 600 W untuk 20 minit dalam keadaan berasid (pH 1.3) adalah TiO₂ yang terdop sendiri (Ti³⁺ ion). Tambahan pula, TiO₂ yang berkonjugat dengan N-GQDs telah disediakan melalui kaedah dua-bekas hidroterma dengan muatan optima 3 mL titanium(IV) isopropoksida (TTIP). Bagi N-GQDs/TiO₂ NK, anjakan dalam jurang tenaga (1.53 eV) telah menonjol apabila pemuatan TTIP meningkat sambil mengekalkan struktur hablur tetragon anatase yang mempunyai purata saiz partikel 11.46 ± 2.8 nm. Selain itu, penilaian sitotoksiti menunjukkan bahawa kepekatan bahan nano yang selamat adalah daripada 0.01 mg/mL hingga 0.5 mg/mL sepertimana kebolehidupan sel menurun secara mendadak pada 1.0 mg/mL. Setelah pengaktifan foto N-GQDs/TiO₂ NK dengan cahaya inframerah terdekat, nanokomposit tersebut menghasilkan spesies oksigen reaktif (ROS) terutamanya oksigen singlet (¹O₂) yang mengakibatkan kematian sel yang ketara dalam sel MDA-MB-231 berbanding dengan sel HS27. Pengaktifan Caspase Glo-3/7 menunjukkan sel yang telah dirawat mengalami jalur kematian sel berdasarkan apoptosis. Di samping itu, disrupti potensi membran mitokondria yang berlaku dalam sel mencadangkan bahawa rawatan PDT bermediasi N-GQDs/TiO₂ lebih mendorong kepada apoptosis bersandarkan mitokondria. Dengan itu, kebolehan nanokomposit berasaskan titanium dioksida dalam mencapai hasil seluler yang diinginkan setelah pengaktifan foto membuktikan ia mempunyai potensi yang baik sebagai fotosensitiser dalam PDT untuk rawatan kanser payudara.

**SYNTHESIS AND CHARACTERISATION OF N-DOPED GRAPHENE
QUANTUM DOTS/TITANIUM DIOXIDE NANOCOMPOSITE AS
PHOTOSENSITISER IN PHOTODYNAMIC THERAPY FOR BREAST
CANCER TREATMENT**

ABSTRACT

Titanium dioxide nanoparticles (TiO₂ NPs) have been proven to be a potential candidate in cancer therapy, particularly in the application of photodynamic therapy (PDT). However, the application of TiO₂ NPs is limited due to the fast recombination rate of electron (e⁻)/hole (h⁺) pairs attributed to their wider bandgap energy. Thus, surface modification is explored to shift the absorption edge to a longer light wavelength to allow penetration into deep-seated tumours. In this study, TiO₂ NPs conjugated with N-doped graphene quantum dots composites (N-GQDs/TiO₂ NCs) to extend the light absorption properties of TiO₂ to longer near-infrared (NIR) wavelengths. A facile one-pot hydrothermal method was employed to synthesise N-GQDs with an average particle size of 4.40 ± 1.5 nm at optimum conditions with molar ratio citric acid (CA):ethylenediamine (EDA) (1:1) at 180 °C for 4 h and primary amine (EDA) as the N-precursors. The blue emissive N-GQDs have photoluminescence (PL) quantum yield of 80.2 %, exhibited excitation-independent PL emission at 442 nm, with an excitation wavelength of 340 nm. Whereas, the anatase TiO₂ NPs were synthesised using microwave-assisted synthesis in the aqueous phase with an average particle size of 11.46 ± 2.8 nm, a small crystallite size (12.2 nm) and low bandgap energy (2.93 eV). Based on the X-ray photoelectron spectroscopy (XPS) analysis, it was found that the square-shaped TiO₂ NPs

synthesised at 600 W for 20 min under acidic conditions (pH 1.3) are self-doped TiO₂ (Ti³⁺ ions). Furthermore, the TiO₂ conjugated with N-GQDs were prepared *via* a two-pot hydrothermal method with an optimum 3-mL loading of titanium(IV) isopropoxide (TTIP). For the N-GQDs/TiO₂ NCs, the shifting in the bandgap energy (1.53 eV) was prominent as the TTIP loading increased while persisting anatase tetragonal crystal structure with an average particle size of 11.46 ± 2.8 nm. Besides, the cytotoxicity assay showed that the safe concentration of the nanomaterials was from 0.01 mg/mL to 0.5 mg/mL as the cell viability decreased prominently at 1.0 mg/mL. Upon the photo-activation of N-GQDs/TiO₂ NCs with NIR light, the nanocomposites generated reactive oxygen species (ROS) were mainly singlet oxygen (¹O₂) that caused more significant cell death in MDA-MB-231 than in HS27 cells. The activation of Caspase Glo-3/7 indicated that the treated cells undergo an apoptosis-based cell death pathway. Moreover, the mitochondrial membrane potential disruption has occurred in the cells further suggested N-GQDs/TiO₂-mediated PDT treatment induced mitochondrial-dependent apoptosis. As such, the capability of the titanium dioxide-based nanocomposite in achieving desirable cellular outcomes upon photo-activation proved that it has good potentials as a photosensitiser in the PDT for breast cancer treatment.

CHAPTER 1

INTRODUCTION

1.1 Overview

Breast cancer owes the high mortality rates among women around the world with nearly two million new cases reported in 2018. According to the statistics from 2012-2016, breast cancer accounted for 34.1 % of all cancers among women in Malaysia which has increased by 2 % as compared to the report from 2007-2011 (32.1 %) (Azizah et al., 2019). The mortality rates due to breast cancers have increased in Southeast Asia, particularly in Malaysia and Thailand (Youliden et al., 2014). The chance of retaining cancer-inflicted breast on a cancer patient depends on the stage at which the disease is detected. Approximately 1 in 19 Malaysian women are at risk with breast cancer every year, where almost 50 % of those affected are under 50 years of age (Azizah et al., 2019). Traditional therapies such as surgery, chemo- and radiation therapy lead to severe side effects that reduce patients' quality of life.

Among the emerging cancer therapy methods, photodynamic therapy (PDT) has been explored currently. PDT involves the utilisation of photosensitising agent, oxygen and a light source that causes irreversible damage to the cancerous tumour cells by inducing a sequence of photochemical and photobiological processes (Li, 2013). Tumour-localising photosensitisers are administered to the targeted area *via* topical, intravenous injection or oral application. After a certain period, the photosensitising agent is absorbed by the tumour cells. This duration is known as drug-to-light-interval. Then, the light of a specific wavelength is used to irradiate at the targeted area to activate the photosensitising agent. Upon activation, the

photosensitising agent generates reactive oxygen species (ROS) which then causes cell death *via* apoptosis, necrosis, or autophagy depending on the nature of photosensitiser, type of cells, the incubation protocol and the intensity of light employed (Wiegell et al., 2012).

The effective use of PDT depends on the type of photosensitising agents employed. Numerous inorganic and organic materials such as cadmium selenide, CdSe, Chlorin e6, Ce6, and hypocrellin A, HA (inorganic) (Huang, 2005), and porphyrin-based materials (organic) (Lin et al., 2020) have been explored as photosensitising agents in PDT for cancer treatments. Limitations of most existing porphyrin-based PDT are its poor water dispersibility and photostability. Therefore, they are easily accumulated under physiological conditions, severely lowering the quantum yields of ROS production. Other drawbacks of most current PDT agents include the inability to absorb at longer wavelengths (>700 nm) which restricts the light penetration, especially for bulky tumours. Moreover, the applications of such materials in clinical trials have been hampered by the imprecision of their cell-killing potential. This leads to undesirable toxicity, potentially causing damage to both cancer and non-cancerous cells/tissues.

In recent years, scientists have focused on research on nanotechnology molecules as PDT agents that exhibit anti-cancer activity, and progress has been made to the relevant pharmacotherapeutic field. In general, nanotechnology can be defined as the employment of engineering, chemical, and biological approaches on materials at the atomic level, with dimensions in the range of 1-100 nm. Nanostructured materials have been attracting a great deal of attention in PDT as they exhibit peculiar properties that differ significantly from those of their bulk

particles. These properties led to the advancement in selectivity, sensitivity and reliability over classic photosensitisers. Upon administration, nanoparticles-based drugs are preferentially taken up and accumulate at the tumour sites due to the enhanced permeability and retention (EPR) effect (Lucky et al., 2015). Thus, it offers an effective method to precisely locate and cause tumour cell destruction simultaneously, preventing overdose of photosensitisers and precisely control treatment duration. Among the nanomaterials, metal oxides have received broad attention due to their distinguished properties than other types of nanoparticles (Roy et al., 2003).

In the diverse nanomaterial community, metal oxide nanoparticles have the advantages of generating reactive oxygen species (ROS), resulting in cell death, in the presence of light illumination (Wang et al., 2004). Non-biodegradable metal oxide nanoparticles generally have good reusability as a photocatalyst. Acting as a photosensitiser or nanocarrier, metal oxides exhibit relatively good stability as compared to existing organic nanoparticles, with regard to temperature and pH change. Moreover, the surface properties of metal oxides can be easily modified *via* surface functionalisation or coating. Among the existing metal oxide nanoparticles, titanium dioxide (TiO₂) has attracted great research interest as photosensitisers for PDT. As an inorganic photosensitiser, it is more stable than classic organic photosensitisers in performing PDT. This trait is attributed to the nanoscale size and anti-photodegradable stability of TiO₂. Despite their excellent performance as a photosensitiser, concerns about their potential toxicity have been raised. Although, some literature studies reported TiO₂ is not toxic to human cells, it still an obstacle for their application in PDT (Ghosh et al., 2010; Hou et al., 2019). Furthermore, the

activation of pristine TiO₂ is triggered upon shorter wavelength UV light irradiation to generate ROS.

To overcome the shortcomings of TiO₂, incorporating TiO₂ with quantum dots (QDs) have been identified as a potential approach. QDs have unique tunable optical and emission properties that depend on their particle size (Li & Yan, 2010). Modifying surface properties of TiO₂ with QDs will assist in extending the light absorption properties of TiO₂ to longer wavelengths. Additionally, this will allow deeper penetration into tissues. Besides, QDs provide great photodynamic therapeutic potential as it is a strong light absorber due to its large transition dipole moment. In PDT, QDs possess dual-function nature as an energy transducer and carriers of photosensitisers (Tabish et al., 2018). Therefore, utilisation of carbonaceous material, N-GQDs to modify TiO₂ surface has great research interest. Besides, heteroatom doping (N atom) of GQDs results in high quantum yield, good stability and higher catalytic activity by tuning their electrochemical properties (Li et al., 2012). Good biocompatibility properties of N-GQDs will help to reduce the present toxicity of TiO₂ and which warrants further exploration in PDT as the photosensitisers should be non-toxic in the absence of light illumination (Ramachandran et al., 2020). Furthermore, as a carrier, N-GQDs ensure precise localisation of the potential N-GQDs/TiO₂ NCs at the site of the tumour and therefore, avoiding harm to non-cancerous cells. Thus, the incorporation of TiO₂ with N-GQDs holds great promise in PDT.

Herein, the main aim of this study is to develop new N-GQDs/TiO₂ NCs as a good candidate for photosensitising agents for PDT with good therapeutic potential.

1.2 Problem statement

TiO₂ NPs have great potential in PDT over classic photosensitisers and other nanoparticles. However, pristine TiO₂ can only be activated under UV light irradiation. Generally, short-wavelength UV light has poor tissue-penetrating capability besides disrupting DNA structure by forming radicals which led to dangerous health consequences such as premature skin ageing that promotes skin cancer, acute photokeratitis, other cellular damage. Some researchers claimed self-doped TiO₂ NPs can absorb visible light which is caused by their surface defects. Furthermore, existing classic photosensitisers exhibit poor selectivity towards tumours cells and highly accumulated on the skin which causes photosensitivity. Moreover, they have absorption maxima at wavelengths in the visible region (~630 nm) which limits their tissue penetration depth. This is because the visible light spectrum is strongly absorbed by most of the tissue chromophores such as melanin, fat and haemoglobin. This will lead to incomplete treatment and tumour relapse if the tumour is located in deeper locations. Thus, light stimulus with wavelengths in the NIR range (700-1300 nm) would be beneficial in improving the penetrability of the PDT agent when administered in solid or deep-seated tumours, for instance, breast tissue. Besides, the potential toxicity of TiO₂ NPs hampers their application in PDT as the International Agency for Research on Cancer has classified TiO₂ NPs as a group 2B carcinogen. As a photosensitiser, it must be non-toxic or must not degrade to release toxic degradation products without light activation. Therefore, this is made possible by incorporating N-GQDs that modify the surface properties as well as mitigate the toxicity of pristine TiO₂ due to its unique physicochemical properties and dual-function nature in PDT. The N-GQDs with good biocompatibility

properties improve the dispersibility of the TiO₂ in the nanocomposite. The nanoscale size of the N-GQDs based TiO₂ PDT agent ensures precise localisation of the potential drug at the tumour site without causing significant harm to the healthy cells.

1.3 Research objectives

The objectives of this research are as follows:

- i. To synthesise and characterise the N-GQDs, TiO₂ NPs, N-doped graphene quantum dots/titanium dioxide nanocomposites (N-GQDs/TiO₂ NCs).
- ii. To determine characteristics of N-GQDs, TiO₂ NPs and N-GQDs/TiO₂ NCs in cell culture medium and their potential cytotoxicity to the MDA-MB-231 and HS27 cell line.
- iii. To evaluate the *in vitro* photodynamic activity of N-GQDs/TiO₂ NCs on MDA-MB-231 cell line.
- iv. To investigate the possible mechanism of ROS generation by N-GQDs/TiO₂ NCs upon near-infrared light irradiation.

1.4 Outline of the thesis

The thesis consists of six chapters:

Chapter 1 is an overview of the study. It emphasises the problem statements, research objectives and outlines of the content.

Chapter 2 is a detailed literature review on some basic knowledge nanotechnology in biomedical applications, photodynamic therapy and properties of TiO₂ NPs and N-GQDs.

Chapter 3 outlines the general methodology used for this study. Firstly, experimental techniques and design for preparing N-GQDs, TiO₂ NPs, and N-GQDs/TiO₂ NCs were detailed out. Besides, experimental procedures employed for *in vitro* photodynamic therapy are discussed. The principles of the instrumental characterisation methods by Fourier transform infrared (FTIR), X-Ray diffraction (XRD), X-ray photoelectron spectroscopy (XPS), high-resolution transmission electron microscopy with selected area electron diffraction (HRTEM/SAED), ultra-visible spectrometer (UV-Vis), field emission scanning electron microscope (FESEM), photoluminescence spectroscopy (PL) and hydrodynamic size – zeta potential analysis are briefly discussed.

Chapter 4 summarise the synthesis and optimisation studies of N-GQDs, TiO₂ NPs and N-GQDs/TiO₂ NCs. Characterisations of N-GQDs, TiO₂ NPs and N-GQDs/TiO₂ NCs were also discussed.

Chapter 5 presents the characterisation of N-GQDs, TiO₂ NPs, and N-GQDs/TiO₂ NCs in cell culture medium and their respective cytotoxicity assay on MDA-MB-231 and HS27 cell lines. Also, discusses results and discussion of *in vitro* photodynamic therapy using N-GQDs/TiO₂ NCs on both cell lines.

Chapter 6 presents the conclusion of the study and provides recommendations for future work.

CHAPTER 2

LITERATURE REVIEW

2.1 Nanotechnology in biomedical applications

A plethora of research has been conducted in the past decades on the application of nanoparticles in biomedical applications. Nanoparticles are described as particles with a size in the range from 1-100 nm. These ultra-small size particles have been considered to offer numerous advantages as compared to bulk particles. This is due to their unique properties such as nanoscale size, tunable optical properties, high specific surface area, enhanced magnetic properties and attractive mechanical properties (Issa et al., 2013; Das et al., 2013). The types of nanoparticles extensively applied in biomedical applications are metallic nanoparticles, metal oxide nanoparticles, magnetic nanoparticles, and quantum dots. These different types of nanoparticles are being used in a blend of various applications, for instance, biosensors, bioimaging, targeted drug delivery, hyperthermia treatment, tissue engineering, photodynamic and sonodynamic therapy (Issa et al., 2013).

Metallic nanoparticles are generally generated from are gold, silver, copper, platinum, selenium, gadolinium and palladium. Among these, the most commonly used metallic nanoparticles are gold and silver. Gold nanoparticles (GNPs) have unique size and shape-dependent optical and electronic properties, good biocompatibility and ease of surface functionalisation, enabling them to be used in biosensing, bioimaging and photothermal therapy (Li et al., 2010). Moreover, due to their negative surface charge, GNPs can be easily functionalised with organic molecules which allows the conjugation with antibodies, ligands and drug molecules for targeted drug delivery system. Besides, silver nanoparticles (Ag NPs) possess

similar unique physicochemical properties as GNPs with additional antibacterial, antifungal and anti-inflammatory properties (Qing et al., 2018). These properties have led their usage in antimicrobial and disinfectant applications, which are mainly applied in the medical industry, wound dressing, food industry and device coatings. Although GNPs and Ag NPs do not exhibit fluorescence properties, surface plasmon resonance of these nanoparticles can be employed to enhance biological *in vitro* and *in vivo* imaging (Lee & El-Sayed, 2006).

Apart from metallic nanoparticles, metal oxide nanoparticles also have attracted considerable interest in biomedical applications. The most widely used metal oxide nanoparticles are titanium dioxide (TiO₂), zinc oxide (ZnO), cerium oxide (CeO₂) and mesoporous silica nanoparticles (MSNs). Besides good biocompatibility, chemical stability, low toxicity, TiO₂ and ZnO nanoparticles possess unique photocatalytic properties that could be utilised in sonodynamic and photodynamic therapies for cancer treatment (Bogdan et al., 2017). Both nanoparticles could be triggered with the aid of ultrasound stimulation or light irradiation, resulting in the production of reactive oxygen species (ROS) which induces cancer cell death. Moreover, intrinsic fluorescent properties and large surface area with versatile surface chemistry of ZnO enable their application *in vitro* and *in vivo* cellular imaging and drug delivery applications, respectively (Xiong, 2013). Besides, cerium oxide (CeO₂) has gained much attention as a biosensor due to its high oxygen storage capacity and adsorption capability, enhanced mechanical strength and high isoelectric point. The positive surface charge of CeO₂ can be employed to bind with negatively charged biosensing molecules (Patil et al., 2012). Additionally, studies on MSNs have shown the ability of these nanoparticles to

deliver chemotherapeutic drugs to different cancer cells *in vivo* and *in vitro* levels. Thus, silica nanoparticles act as multifunctional drug-delivery agents (Rahikkala et al., 2018).

Furthermore, interest in magnetic nanoparticles has grown rapidly and their applications in the biomedical field have gained research attention in recent years. Generally, materials that exhibit high saturated magnetisation are metal (iron (Fe), cobalt (Co), nickel (Ni)) and metal oxides (Fe_3O_4 , $\gamma\text{-Fe}_2\text{O}_3$). However, pure metals possess toxicity and can be oxidised easily. Unlike pure metals, maghemite ($\gamma\text{-Fe}_2\text{O}_3$) and magnetite (Fe_3O_4) are more biocompatible, less sensitive to oxidation and relative ease of surface modification (Couto et al., 2015). The appropriate coating with polymers (polyethylene glycol (PEG), polyvinyl alcohol (PVA)), functional groups (carboxyls, amines and thiols) and doping with magnetically susceptible elements (Fe, Co, Mn), enables these nanoparticles to achieve colloidal stability, longer blood circulation time, reduce aggregation and prevent oxidation (Sabale et al., 2015). In general, iron oxide nanoparticles have been extensively used in targeted drug delivery, magnetic hyperthermia, tissue engineering and as a contrast agent in magnetic resonance imaging (MRI). Moreover, nanoparticles with superparamagnetic properties such as superparamagnetic iron oxide nanoparticles (SPIONs) exhibit the combination of high magnetic susceptibility and no remanence at room temperature. These properties enable their utilisation *in vivo* magnetic hyperthermia treatment and MRI applications (Revia & Zhang, 2016). These nanoparticles also can be used to precisely locate drugs and genes at the targeted area with the influence of an external magnetic field. Besides, bimetallic or alloy nanoparticles (Fe-Co, Fe-Ni, iron-platinum (Fe-Pt) and copper-nickel (Cu-Ni))

possess superparamagnetism, high coercivity, good Curie temperature, biocompatibility, high chemical stability and saturation magnetisation and are extensively used in biomedical applications (Hayashi et al., 2013).

In addition to the existing type of nanoparticles, quantum dots which are also known as semiconducting nanoparticles emerged as a promising candidate in bioimaging, drug delivery and biosensor (Matea et al., 2017). Quantum dots belong to the class of nano-sized crystals having dimensions of 1-10 nm with superior mechanical and physicochemical properties. Quantum dots (QDs) are among the most widely used nanoparticle in optical imaging due to their optical properties that can be tuned by varying their size, which can be utilised for labelling tissues and biomolecules. Besides, as compared to traditionally used organic dye molecules, semiconductor quantum dots have 100-fold fluorescence brightness, low toxicity, high quantum yield, broad excitation and narrower emission spectra. Resistant to degradation and longer-lasting photostability of quantum dots allows cellular process tracking for an extended period (Walling et al., 2009). The application of quantum dots in a targeted drug delivery system has significant advantages including longer circulation time, controlled release of drugs, high drug-loading capacity and ability to integrate multiple targeting ligands on their surface. Quantum dots can play multiple roles as they have imaging and targeting potential simultaneously in the drug delivery system (Bajwa et al., 2016). Moreover, quantum dots are commonly used as optical indicators in biosensors. As a luminescent marker, they are used in detecting targeted biomolecules. Detection and imaging of tumour cells by these quantum dots enhances their potential for the diagnosis of cancer in their early stage

with precise estimation and visual tracking of tumour elimination and reduction (Fang et al., 2012).

2.2 Nanomaterials in Photodynamic Therapy

Photodynamic therapy (PDT) is an emerging non-invasive, clinically approved and localised therapy for cancer treatment. The principle of PDT is based on the accumulation of photosensitisers in the tumour which absorb and convert light of an appropriate excitation wavelength into a generation of ROS to kill the cancer cells (Li, 2013). The latter reaction occurs following type I and type II reactions as shown in Figure 2.1. In Type 1 reaction, the direct interaction of excited photosensitiser with macromolecules results in the formation of the radicals, which then interact with oxygen to produce ROS. Meanwhile, in type II reaction, the energy transfer between activated sensitiser and oxygen will be generating singlet excited state of oxygen (1O_2) (Pass, 1993).

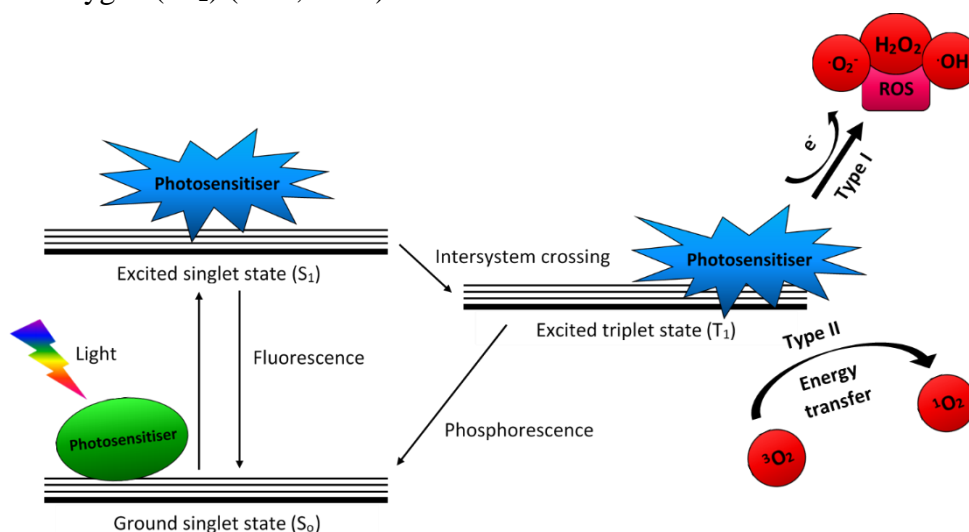


Figure 2.1: Type I and type II reaction mechanism of ROS generation in PDT.

The effectiveness of PDT depends on the type of photosensitising agents employed. The first generation of photosensitiser that arose in the 19th century is hematoporphyrins (Hp). Initially, it was used as a fluorescent diagnostic tool for

cancer diseases, but it requires higher doses to obtain desired results due to its heterotypical nature. Further purification of Hp, resulted in the formation of porfimer sodium (photofrin). It was used in the clinic to treat pre-cancers and cancers and it was authorised by U.S Food and Drug Administration (FDA) and the European Medicine Agency (EMA) (van Straten et al., 2017). However, the complex mixture of photofrin molecules have low light absorption and poor tumour selectivity, thus, led to the development of the second generation of photosensitiser (Sun et al., 2016). They were designed to achieve better tumour selectivity, reduce the dosage of drugs used and able to absorb light at a longer wavelength. Second generation photosensitisers consist of porphyrin or porphyrin-based derivatives such as chlorins, texaphyrins, phthalocyanines, pheophorbides, bacteriopheophorbides, and including nonporphyrinoid compounds (O'Connor et al., 2009). Besides, modified second-generation photosensitisers are known as third-generation photosensitisers (Josefsen & Boyle, 2008). They are modified with biologic conjugates such as antibodies or liposomes, carriers and peptides to enhance their therapeutic efficacy. Thus, they can precisely target the tumours, have better penetrability and minimise the side effects by using a lower dosage of photosensitisers.

The use of nanoparticles in PDT enhances PDT efficacy. Nanoparticles in PDT have been categorised as active and passive nanoparticles based on the absence and presence of targeting ligands on the surface (Chatterjee et al., 2008). Active nanoparticles are used as 'active participant' in the excitation of photosensitiser. They can be sub-classified based on the activation mechanism into photosensitiser nanoparticles, upconversion nanoparticles and self-lighting nanoparticles. Photosensitiser nanoparticles (CdSe QDs, fullerenes, TiO₂ and ZnO) can generate

ROS on their own without a mediating photosensitiser molecule (Samia et al., 2006; Liu et al., 2007; Finegold & Cude, 1972). Furthermore, upconversion nanoparticles (UCN) are nanoscale composites that convert lower energy radiation into higher energy light. These nanocomposites also are commonly known as upconverting phosphors (UCPs) ($\text{NaYF}_4:\text{Yb}^{3+},\text{Er}^{3+}$), which are comprised lanthanide-based ceramic particles in the submicrometer size range (Qian et al., 2009). They emit visible light by absorbing NIR or infrared light. Apart from that, self-lighting nanoparticles are employed in Self-Lighting Photodynamic Therapy (SLPDT) which combines radiation therapy and PDT, without using an external light source. This therapy employs scintillation luminescent nanoparticles ($\text{BaFBr}:\text{Eu}^{2+}, \text{Mn}^{2+}$ and $\text{LaF}_3:\text{Tb}^{3+}$) loaded with photosensitisers as PDT agents (Lucky et al., 2015). Meanwhile, passive nanoparticles are defined as ‘passive carriers’ of photosensitisers in PDT. They act as delivery vehicles to further enhance drug loading efficiency, bioavailability, controlled drug release and degradation rate. These nanoparticles are sub-categorised based on material composition into biodegradable and non-biodegradable nanoparticles. Polylactide (PLA), polyglycolide (PGA), and their copolymer poly(D,L-lactide-co-glycolide) (PLGA), polysaccharides and proteins are among the synthetic polymers used widely for the preparation of biodegradable nanoparticles as drug carriers (Calixto et al., 2016; Lucky et al., 2015). Besides, GNPs, SPIONs and ceramic-based nanoparticles are employed for PDT to develop a non-biodegradable-based drug delivery system. Non-biodegradable nanoparticles differ from biodegradable nanoparticles as they do not degrade and release drugs in a controlled manner (Roy et al., 2003; Wieder et al., 2006; Munnier et al., 2011).

2.3 Titanium dioxide (TiO₂)

2.3.1 General

As a naturally occurring oxide form of titanium, TiO₂ has been widely explored in recent years. It is an n-type semiconductor and belongs to the transition metal oxides family. The special characteristics of TiO₂ are directly connected to its crystal structure that is closely related to its synthesis method (Nyankson et al., 2013). Notably, TiO₂ is being produced extensively as it possesses numerous unique properties such as low toxicity, photoactive, excellent stability, inexpensive, high photo/chemical corrosion resistance, long durability, biological and chemical inertness (Vadlapudi et al., 2013).

In the early twentieth century, TiO₂ was used in paints as a substitute for white dye. Since then, extensive research efforts performed by researchers on TiO₂ and its potential applications. Due to its improved thermal stability, strong UV absorption and excellent pigmentary properties, it is commonly used for heterogeneous catalysis, photoelectrochemical conversion, purification of water and air, self-cleaning coating surfaces, water splitting, electro-ceramics, glass and also, as a non-toxic food additive authorised by European Union (Pelaez et al., 2012). Besides, it also acts as an excipient in the pharmaceutical applications to produce cosmetics sunscreens and their white pigments used in plastics as a colourant (Skocaj et al., 2011).

2.3.2 Chemical structure and properties

There are two most common crystallographic phases of TiO₂, which are anatase and rutile, while brookite form is rather rare, as shown in Figure 2.2.

- 1) Anatase: It is a tetragonal crystallographic polymorph of TiO_2 . The anatase structure is made up of octahedra four sharing corners (vertices) which form (001) planes. When compared to the rutile phase, the distortion of the anatase TiO_6 octahedron is slightly larger.
- 2) Rutile: It is the primary source of TiO_2 and becomes the most stable polymorph at most temperatures and pressures. For the rutile phase, the octahedra two sharing edges at (001) planes result in a tetragonal structure.
- 3) Brookite: It possesses an orthorhombic crystal structure. It is composed of 8 atoms per unit cell of TiO_2 and is formed by sharing TiO_6 octahedra edges and corners.

TiO_2 is a semiconductor with bandgap energy large than 3.0 eV (3.2 for anatase, 3.0 for rutile, and ~ 3.2 eV for brookite), thus, pure TiO_2 is primarily active upon UV irradiation. Anatase structure is the preferred crystal polymorph over rutile and brookite, although rutile TiO_2 exhibits a relatively narrower bandgap and higher stability than anatase. This is due to its lower density, higher electron mobility and a slower rate of recombination of e^-/h^+ pairs when compared to the rutile phase (Kandiel et al., 2013). On the other hand, brookite is a minimally explored phase in experimental investigations as it is the least active phase of TiO_2 . Brookite TiO_2 has a complex crystalline structure, higher cell volume and lowest density than other polymorphs and therefore, it is not commonly studied (Di Paola et al., 2013).

Furthermore, amorphous TiO_2 can be transformed into a crystalline phase (anatase or brookite) *via* the calcination process which takes place at approximately 400 °C. It can further convert from one phase to another phase, depending on the processing temperature applied. Anatase and brookite can converted to

thermodynamically stable and poorly active rutile when the processing temperature exceeds 600 °C. The other factors that influence this phase transformation including conditions and precursors used during preparation, levels of oxygen vacancies, impurities present and primary particle size of the anatase phase (Bianchi et al., 2016).

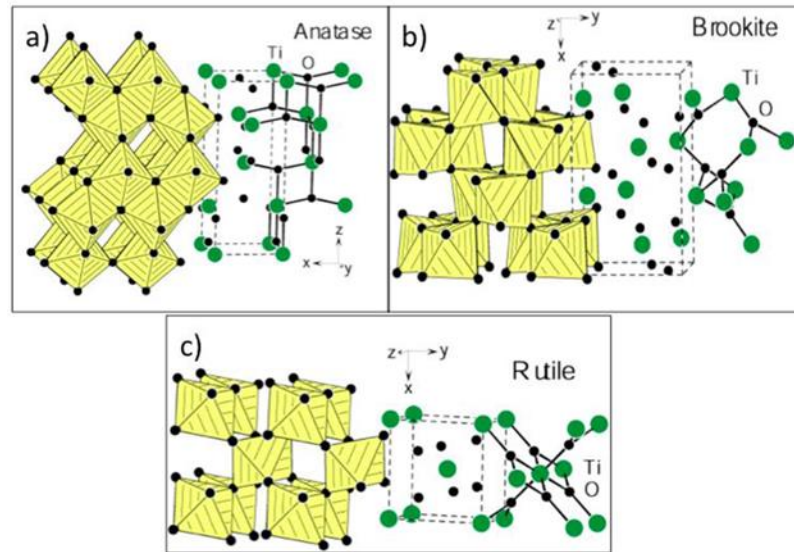


Figure 2.2: Bulk crystalline structures of the (a) anatase, (b) brookite and (c) rutile type TiO_2 (Bianchi et al., 2016).

Several conventional methods such as hydrothermal method, solvothermal method, sol-gel method, direct oxidation method, chemical vapour deposition, sonochemical method and microwave-assisted synthesis are employed, as shown in Table 2.1. Among these, the hydrothermal route is easy and environmentally friendly. However, it requires a longer reaction duration which could result in morphological changes of nanoparticles (Liu et al., 2014). On the other hand, microwave-assisted synthesis has an advantage of rapid heat transfer with shorter reaction time and higher reaction rate, selective heating, excellent control of experimental parameters and yield as compared to the conventional heating methods.

Table 2.1: TiO₂ NPs synthesis method, reaction conditions and their respective outcome.

Method	Reaction conditions	Synthesis outcome	Reference
Hydrothermal	TTIP + acetylacetone + ethanol + urea (in DI water) (150 °C for 18 h)	anatase phase, particle size ~24 nm, bandgap 3.09 eV	Thapa et al., 2012
Solvothermal	TTIP + ethanol + H ₂ SO ₄ (90 °C for 12 h)	anatase phase, particle size ~4 nm, bandgap 3.01 eV	Ramakrishnan et al., 2018
Sol-gel	TTIP + starch solution + NH ₄ OH (85 °C for 30 min)	anatase phase, particle size ~64 nm, bandgap 3.00 eV	Muniandy et al., 2017
Direct oxidation	Ti metal plate + H ₂ O ₂ solution + NaF (353 K for 72 h)	anatase phase TiO ₂ nanorods, ~30 x 40 nm	Wu, 2004
Chemical vapour deposition	TiCl ₄ (in dichloromethane) + substrates (KCl crystal, KBr pellet, Al foil and freshly sliced MICA) (320 °C)	grain sizes of TiO ₂ /KCl (6.4 nm, anatase), TiO ₂ /Al (7.9 nm, anatase + brookite), TiO ₂ /KBr (8.3 nm, anatase), TiO ₂ /MICA (17.9 nm, anatase)	Djerdj et al., 2005
Sonochemical	TTIP + isopropanol + acetic acid (40- minute sonication)	anatase phase, particle size 19.9 nm, bandgap 3.25 eV	Swapna & Haridas, 2016
Microwave	TTIP + HNO ₃ (180 °C for 20 min)	anatase (major) + brookite (minor) phase, particle size 7 - 28 nm, bandgap 3.1 eV	Falk et al., 2018

2.3.3 Application of TiO₂ in the biomedical field

Previous studies have demonstrated TiO₂ as a promising candidate for various biomedical applications, owing to their unique photocatalytic properties, excellent biocompatibility, high chemical stability, low toxicity, intrinsic properties and versatile fabrication techniques. Among all the applications, the most common biomedical applications of TiO₂ are photodynamic therapy for cancer, drug delivery system, cell imaging and biosensors.

Photodynamic therapy is a treatment that uses photosensitiser together with a specific type of light to kill cancer cells. TiO₂ NPs are designed to be used as photosensitising agent in PDT attributed to their nanoscale size, they possess the ability to produce ROS. When TiO₂ NPs are irradiated with energy equal or greater than the bandgap of TiO₂ (3.20 eV), the electrons (e⁻) in the valence band (VB) of TiO₂ are excited to the conduction band (CB), creating positive holes (h⁺) in the VB. This leads to the redox reaction on the surface of these semiconductor nanoparticles. The excited electrons and the holes further undergo redox reaction with oxygen and water molecules to produce superoxide anions (O₂⁻), singlet oxygen (¹O₂), hydrogen peroxide (H₂O₂) and hydroxyl radicals (·OH) (Linsebigler et al., 1995; Kang et al., 2019). The generated ROS causes detrimental effects on targeted cells. However, the poor solubility of TiO₂ NPs in an aqueous medium limit their application in PDT. As such, Seo and co-researchers employed a high-temperature non-hydrolytic method to synthesise TiO₂ NPs soluble in water (Seo et al., 2007). The fabricated nanoparticles exhibited significant toxicity on human melanoma cells (A375) upon illuminated with UV irradiation than Degussa P-25 nanoparticles. Besides, to overcome the rapid recombination of e⁻/h⁺, surface modification of TiO₂ NPs with

other elements was developed. In a study by Xu and co-researchers, they loaded gold on the surface of TiO₂ NPs through deposition–precipitation (DP) method (Xu et al., 2007). When Human Colon Carcinoma LoVo cells treated with Au/TiO₂ nanocomposites in the presence of UV irradiation for 100 min, no viable cells were observed at the end of the experiment. However, 60 % of cancer cells were viable when treated with TiO₂ NPs under the same condition.

Another common biomedical application is in the drug delivery system. An ideal drug delivery system to deliver drugs at the targeted site is required to achieve maximised therapeutic efficacy with fewer side effects. Generally, nanoscale materials have a higher surface area which permits maximum drug loading capacity. Various TiO₂ nanostructures such as nanoparticles, capsules, whiskers, nanotubes and porous shapes have been used as a drug carrier to deliver different drugs including temozolomide, daunorubicin, valproic acid, doxorubicin and cisplatin (Yin et al., 2013). TiO₂ based drug delivery system enables efficient drug release, retention of a precise dose of the drug and prolonged exposure to drugs. A notable characteristic of nano-sized TiO₂ is its ability to deliver drugs into the cells in a pH-dependent manner. Tumours often maintain an acidic extracellular microenvironment than that of blood and normal healthy cells. In such circumstances, developing a drug delivery system with the ability to retain the drug when it is transported in the blood circulation at pH approximately 7.4 (neutral and alkaline conditions) but releasing the drug as internalised into tumour cells when pH is less than 7.4 (acidic) were studied extensively (Xu et al., 2015). Daunorubicin-based TiO₂ nanocomposites synthesised with the capability of releasing daunorubicin rapidly in the acidic condition that at pH less than 7.4 (pH 5.0 and 6.0)

(Zhang et al., 2012). The controlled release of daunorubicin from the nanocomposite successfully induced apoptosis in leukaemia cells. Besides, to increase the selective drug action by TiO₂ based drug carrier, TiO₂ are conjugated with the monoclonal antibody. Therefore, this approach increases selectivity towards tumour cells and improves loading capacity specifically for hydrophobic drugs.

In the past few years, TiO₂ has attracted much attention as a potential candidate in cell imaging applications due to its unique chemical active surface. Understanding cell imaging analysis of living cells is important to visualise the structure of the cells and proteins. TiO₂ could be employed in cell imaging *via* fluorescent analysis or MRI by conjugating TiO₂ nanostructures (nanotubes, nanoparticles or nanoprobe) with fluorescent dyes or magnetic contrast agents, respectively. The stated imaging methods are some of the good examples of minimally invasive methods for *in vivo* imaging as compared with X-ray and other imaging methods. Wu and co-workers reported mesoporous titania nanoparticles with good biocompatibility and higher surface area (Wu et al., 2011). The synthesised mesoporous titania nanoparticles were then chemically functionalised with a phosphate-containing fluorescent molecule (flavin mononucleotide). After incubating human breast cancer cells (BT-20) with the latter for 4 h, it resulted in green fluorescence in the cytoplasm, indicating the fluorescent molecules remained inside mesoporous titania nanoparticles throughout the analysis without any significant leaching. As for MRI, Chandran and co-researchers have developed a novel Gd³⁺ doped amorphous TiO₂ as a nano-contrast agent to provide high contrast cancer imaging (Chandran et al., 2011). Since increasing crystallinity of TiO₂ renders lower contrast, amorphous TiO₂ was utilised as a contrast agent. However, Gd-based

contrast agents are not desirable for prolonged retention due to their rapid clearance after 24 h imaging period.

In biosensors, TiO₂ nanostructures are among the most promising material that has attracted significant scientific interest. Biosensors are well-known for their widespread applications such as disease diagnosis, food quality monitoring, environmental monitoring and drug discovery (Li et al., 2009). Various TiO₂ forms such as nanoparticles, nanosheets, sol-gel matrices, nanopores and nanotubes were extensively studied in developing biosensors. These prepared TiO₂ nanostructures present a promising interface to assemble various types of proteins, including antibodies and enzymes. Moreover, the morphology and structure of nano-sized TiO₂ have a significant effect on the property of conjugated enzymes, which ensures the efficiency of the biosensor. Xie and co-researchers have reported TiO₂ nanosheets-based microspheres with a hollow-core shell structure as a biosensor to detect H₂O₂ (Xie et al., 2011). The hollow-core shell structure assists the adsorbed enzyme to immobilise easily on the inner core of microspheres. Thus, it increases the stability and bioactivity of the enzyme resulting in the good performance of the biosensor. As such, TiO₂ based biosensor is a good candidate as a biosensor and it can also be applied in the cell-capture assay to capture targeted cells as the antibodies in the biosensor bind with antigens of targeted cells (Zhang et al., 2012).

2.4 Modification of TiO₂ into TiO₂ nanocomposites

The nanocomposite is defined as a combination or matrix that incorporates different nanoscale materials where one of the materials has a dimension less than 100 nm (Omanović-Miklićanin et al., 2020). Numerous studies have been developed on the modification of TiO₂ into nanocomposites to enhance the performance of the

TiO₂ nanocomposites and fabricate a dual function as the final product. Pure TiO₂ can only be activated using UV light due to its large bandgap energy. Although TiO₂ as a UV absorber is typically adopted for various applications, this appears to be less feasible in terms of utilising photoelectrochemical properties and their potential biomedical applications. Focusing on biomedical applications such as PDT, biosensing and bioimaging, TiO₂ employing UV light irradiation is limited to superficial tumours and it also possesses harmful effects to humans as it damages DNA in host cells and possibly can be carcinogenic upon prolonged exposure. Furthermore, the rapid recombination of photogenerated e⁻/h⁺ pairs significantly limit their photocatalytic activity. Therefore, exhaustive research has been conducted to produce TiO₂-based nanocomposite materials (Ghosh & Das, 2015). In efforts to develop the functional properties of TiO₂, many attempts have been made to incorporate additional components, for instance, polymers, transition metals, metal oxides, noble metals and quantum dots. Moreover, the heterojunctions formed between TiO₂ and other components can shift the light absorption edges of TiO₂ from UV to Vis/NIR wavelength.

Many polymer-based nanocomposites have been synthesised using polymers such as polyethylene glycol, polypropylene, polyester with TiO₂ to extend absorption of TiO₂ to longer wavelength besides to improve biocompatibility by eliminating aggregation (Li et al., 2009). PEGylated TiO₂ NPs exhibited less cytotoxic potency than uncoated TiO₂ (Barkhade et al., 2019). Furthermore, TiO₂ metal oxide was modified with transition metals (Cu, Zn, Fe), metal oxides (ZnO, NiO) and a noble metal (Ag, Pt, Pd) to enhance photocatalytic performances and has higher energy efficiency (Barkhade et al., 2019; Ahmad et al., 2018; Ahamed et al., 2017; López et

al., 2011; Ahamed et al., 2016; Liu et al., 2014; Chan & Shiao, 2008; Latvala et al., 2016). However, these conventional transition metals, metal oxides and noble metals often induce additional toxicity (genotoxicity, inflammation, altered calcium homeostasis) to the nanocomposite. This occurrence is due to their properties of generating ROS by their respective metal ions upon dissociating in the cell culture media. Moreover, the higher cost of noble metals co-catalyst (Pt, Pd) restricts their wide applications.

Since TiO₂ has wider applications in the pharmaceutical field, environmental, food and cosmetic industry, it is crucial to consider toxicity as an important parameter when synthesising TiO₂ based nanocomposite. Thus, modifying TiO₂ metal oxide with quantum dots is more effective due to their unique physicochemical properties. TiO₂ - quantum dots (QDs) composites are extensively used in drug delivery systems, cell imaging and biosensors for biological assays (Ghosh & Das, 2015). Besides, these modified TiO₂ based materials have been explored extensively in environmental applications including dye removal, water and air purification.

A summary of TiO₂ based nanocomposite applied in PDT reaction is tabulated in Table 2.2. Generally, these nanocomposite acts either as a photosensitiser or nanocarrier depending on the absence or presence of active PDT agent.

Table 2.2: TiO₂ based nanocomposite applied in PDT reaction for treating various cancer cells.

Nanocomposite	Function of TiO₂	Light absorption region	Findings	Reference
TiO ₂ NPs conjugated with reduced graphene oxide (RGO-TiO ₂)	Photosensitiser	UV-A/Vis	cell viability of HepG2 cells ~ 30% (UV-A) and ~ 40% (Vis) after 40 min irradiation	Shang et al., 2017
Fe ₃ O ₄ -TiO ₂	Photosensitiser	UV	cell viability ~ 39%	Zeng et al., 2013
ZnPc-TiO ₂	Nanocarrier and to enhance the photokilling effects of ZnPc by improving uptake in the mitochondria or lysosome	Vis	ZnPc-TiO ₂ induced higher phototoxic effects on mammalian cells (Human-derived fibroblasts, THP-1 macrophages, HepG2 cells, Vero cells) than TiO ₂ but less than pure ZnPc. However, ZnPc-TiO ₂ was internalized into the cells at a lower level than free ZnPc	Lopez et al., 2010
N-TiO ₂ -Pc	Nanocarrier and improve cellular uptake efficiency	Vis	N-TiO ₂ -Pc (~ 14% cell viability) exhibited higher photokilling effect on cancer cells (HeLa and KB cells) than Pc (~92% cell viability) due to its highly effective cellular uptake and higher ROS production	Pan et al., 2015